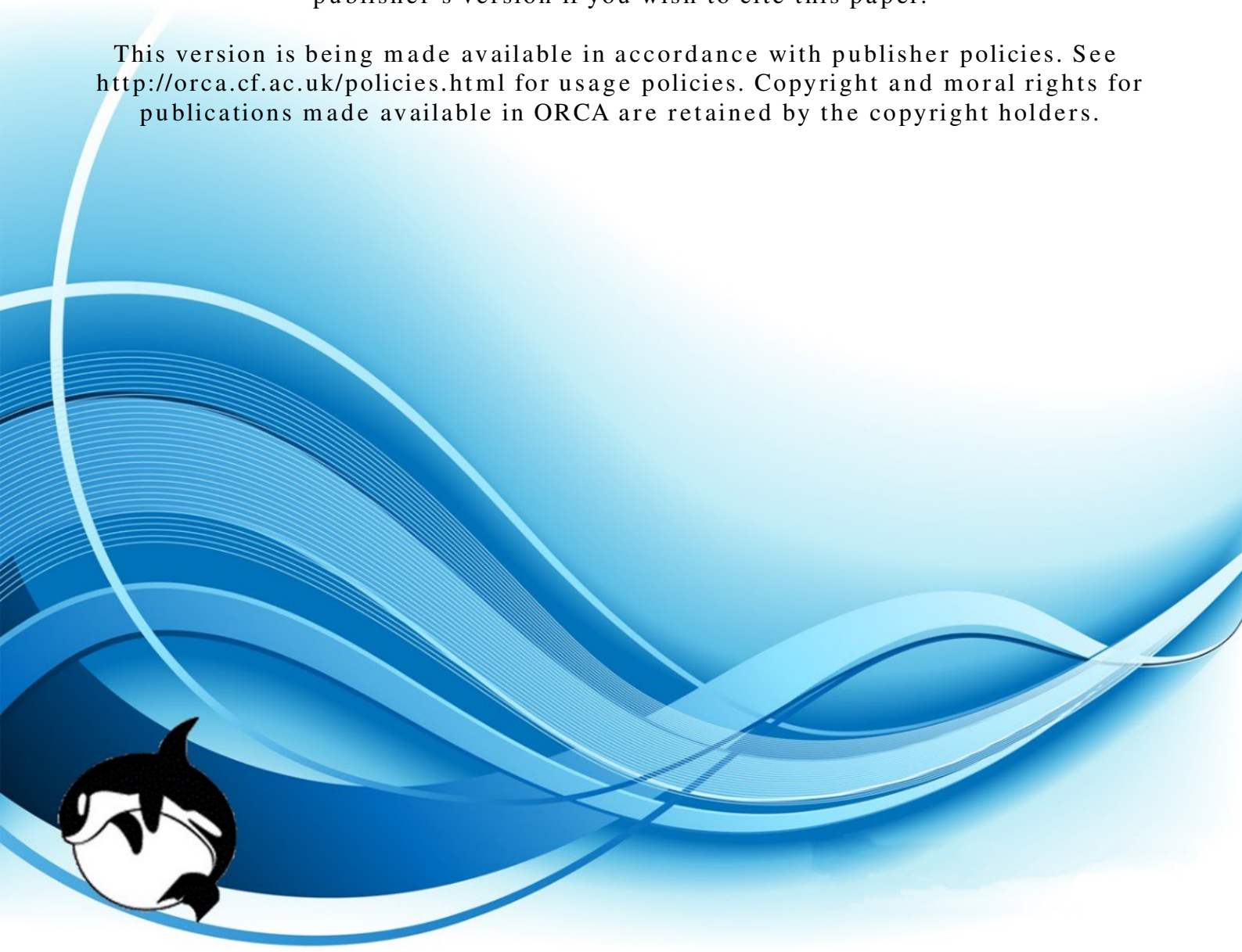

Title: The photocatalytic destruction of cinnamic acid and cinnamyl alcohol: Mechanism and the effect of aqueous ions.

Authors: **Emir Bouleghlimat**[a]

Donald Bethell[b]

Corresponding Author Philip R. Davies[a]

Addresses:

[a]*Cardiff Catalysis Institute, School of Chemistry, Cardiff University, Cardiff CF10 3AT, UK*
daviespr@cardiff.ac.uk

[b]*Department of Chemistry, University of Liverpool, Liverpool L69 3BX, UK*
bethell@liverpool.ac.uk

The photocatalytic destruction of cinnamic acid and cinnamyl alcohol: Mechanism and the effect of aqueous ions.

Emir Bouleghlimat[a]; Donald Bethell[b], Philip R. Davies[a]*

[a]*Cardiff Catalysis Institute, School of Chemistry, Cardiff University, Cardiff CF10 3AT, UK*

[b]*Department of Chemistry, University of Liverpool, Liverpool L69 3BX, UK*

Keywords

Cinnamic acid; photocatalysis; chlorine radicals; mechanism; sulfate; halide

Abstract

Cinnamic acid was chosen as an exemplar molecule to study the effect of potential contaminants on the kinetics and mechanism of the photocatalytic destruction of hydrocarbons in aqueous solutions. We identify the principal intermediates in the photocatalytic reaction of the acid and corresponding alcohol, and propose a mechanism that explains the presence of these species. The impact of two likely contaminants of aqueous systems, sulfate and chloride ions were also studied. Whereas sulfate ions inhibit the degradation reaction at all concentrations, chloride ions, up to a concentration of 0.5 M, accelerate the removal of cinnamic acid from solution by a factor of 1.6. However, although cinnamic acid is removed, the pathway to complete oxidation is blocked by the chloride, with the acid being converted (in the presence of oxygen) into new products including acetophenone, 2-chloroacetophenone, 1-(2-chlorophenyl)ethenone and 1,2-dibenzoylethane. We speculate that the formation of these products involves chlorine radicals formed from the reaction of chloride ions with the photoinduced holes at the catalyst surface. Interestingly, we have shown that the 1-(2-chlorophenyl)ethenone and 1,2-dibenzoylethane products form from 2-chloroacetophenone when irradiated with 365 nm light in the absence of the catalyst. The formation of potentially dangerous side products in this reaction suggest that the practical implementation of the photocatalytic purification of contaminated water needs to considered very carefully if chlorides are likely to be present.

1 Introduction

The high oxidation potential of the radicals produced in aqueous systems by photocatalytic activation at semiconductor surfaces is widely recognised as having great potential for the degradation of water borne contaminants. Investigations have been reported in areas ranging from antibacterial applications to removal of effluent from industrial processes. One example is in the removal of the non-toxic but highly polluting effluent from the palm oil, olive oil and fishing industries. The Malaysian Palm Oil board reports that palm oil mill effluent (POME) is 100 times more polluting than domestic sewage due to its high chemical and biological oxygen demand.[1] The

advantages of highly oxidising chemistry and environmentally friendly processes have led to extensive research in the design and optimisation of systems for the photocatalytic degradation of water borne contaminants.

Whilst a great deal of current photocatalytic research is addressing the central issues of utilising light with frequencies in the visible range and of achieving useful catalytic efficiencies, there are other practical problems to solve. In particular, the application of photocatalysis is likely to be in situations where the target contaminants are accompanied by other species. In this paper, we consider how sulfate and chloride ions might affect the efficiency and reaction pathways of the photocatalytic process, using cinnamic acid as a model substrate since it contains several of the functional groups that are present in the contaminants typically present in effluent from the agricultural industry.[2,3] Both sulfate and chloride ions can lead to the formation of new radicals in solution. In the case of sulfate for example, $SO_4^{\bullet}$ is formed via the radicalisation of HSO_4^- by the $HO^{\bullet}$ radicals created at the catalyst surface.

$$HSO_4^- + HO^{\bullet} \rightleftharpoons SO_4^{-\bullet} + H_2O$$

$SO_4^{\bullet}$ is a strong oxidant and has been shown to have a very different behaviour to that of hydroxyl radicals.[4] Previous studies of the influence of aqueous sulfates on photo-mineralisation processes have found varying effects, for example, Wiszniowski *et al*. found the degradation of humic acid to be initially inhibited in the presence of sulfate, but promoted in later steps by the formation and reaction of $SO_4^{\bullet}$ in solution.[5] Gaya et al.[6] studying a 4-chlorophenol substrate, also found a small increase in the rate of photodecomposition which they attributed to the reactivity of the sulfate radical. Mendez *et al.* discussed the differing behaviour between $SO_4^{\bullet}$ and $HO^{\bullet}$ in the degradation of dodecyl-benzenesulfonate in the presence of fulvic acid;[7] UV/$S_2O_8^{2-}$ degraded the target molecule more quickly than UV/H_2O_2 due to the more specific reactivity of the sulfate radical, therefore reducing the ability for dissolved organic carbon species to scavenge it.

Chloride ions in solution have often been associated with a decrease in photocatalytic oxidation[8] because, like sulfates, they act as scavengers for the hydroxyl radicals, Wang et al.[9] reported that chloride ions had a greater inhibitive effect on the photocatalytic mineralisation of o-methylbenzoic acid than sulfate ions. However, more complex behaviour has also been observed, Piscopo et al. for example showed[10] that, in the photocatalytic decomposition of benzamide and 4-hydroxybenzoic acid over a TiO_2 catalyst, benzamide decomposition is strongly inhibited by the presence of chloride concentrations greater than 0.5 M, whereas the benzoic acid is hardly affected at all. Meanwhile Yang et al.[11] showed chloride decreasing the rate of removal of methylene blue but actually

increasing the rate of removal of 2-naphthol orange. The authors attributed the different effects to the differing extent of adsorption of the two molecules, arguing that the 2-naphthol orange adsorbs more strongly at the TiO_2 surface and is therefore able to react with chloride radicals formed from the interception of the $OH^{\bullet}$ radicals by the chloride ions. Alternative reaction pathways in the presence of chloride have also been observed, with toxic chlorinated byproducts observed in the case of the decomposition of azo dyes in saline wastewater.[12]

In this paper, we have sought to elucidate the effect of alkali-metal sulfates and chlorides on the photocatalytic decomposition of cinnamic acid in water over TiO_2, both in the presence and absence of oxygen. We show how in this system, sulfates act to inhibit the reaction whereas chlorides significantly enhance photooxidation rates and give rise to a number of undesirable products. We explore the role of dissolved oxygen on the reaction mechanism and discuss the photocatalytic decomposition of cinnamic alcohol, benzaldehyde and phenylacetaldehyde as key intermediates on the pathway from cinnamic acid to complete oxidation to carbon dioxide and water.

2 Materials and methods

2.1 Preparation of TiO_2 photocatalyst

Titanium (IV) oxide (Aeroxide® P25, Sigma Aldrich), which is a crystalline powder with particles approximately 21 nm in diameter, composed of ~70% anatase and ~25% rutile and minor amounts of an amorphous phase,[13] was used as the photocatalyst. However, the fine particle size was too small to efficiently filter out and suspended fine particles interfered significantly with UV measurements. Atomic emission spectra (AES) showed that complete removal of titania from the reacting solution was very cumbersome, since the suspended TiO_2 particles could potentially damage the column in the gas chromatography- mass spectrometer system (GC-MS), the P25 was mixed with deionised water up to its incipient wetness point (~1.5 mL per 2 g of powder), and ground into a paste. The paste was dried at 200°C for 2 hours, calcined at 400°C for 3 hours and filtered through a 53 µm sieve. This resulted in a TiO_2 catalyst with excellent photocatalytic properties but particles large enough to be completely filtered out of the reaction.

2.2 Reactor vessel

All experiments were conducted using the UV-LED based photocatalytic test reactor[14,15] developed as part of the EU funded PCATDES project that provides a calibrated adjustable light source and pre-defined test conditions to remove as many sources of uncertainty in photocatalytic analysis as possible and thereby improve data reliability. The test reactor provides a selectable intensity of up to 1.9 kW m^{-2}. The reactor vessel has a 250 mL capacity and is equipped with flowing water cooling. The glass reactor is covered by a purpose-built black plastic covering with

openings designed for several uses including sample taking, temperature control and gas flow. The LEDs are fitted to the top of the black covering providing top down irradiation unhindered by the PCATDES glassware. The reactor sits on top of a magnetic stirrer plate. The total reaction volume was 250 ml , with an initial cinnamic acid concentration of 50 mg L^{-1} at an initial pH of 5. The reaction was carried out in air except those cases where nitrogen sparging is stated. 1 mL liquid aliquots are taken with glass pipettes and filtered into sample vials from which they are added to GC-MS sample vials or diluted for UV absorption measurements. Before every experiment the photocatalyst is allowed to equilibrate in the reaction solution for 30 minutes without light to ensure adsorption of reactants onto the relatively high surface area catalyst is complete before reaction. Longer periods of equilibration were investigated but had no material effect on the reaction.

2.3 Sample analysis

Cinnamic acid concentrations were determined from the molecule's strong absorption at 272 nm and monitored using a Lambda XLS table top UV/Vis spectrophotometer. The error in sample measurement, estimated by repeated measurements, was ~3 µg ml^{-1}. A GCT premier gas chromatograph with an orthogonal acceleration -TOF (time of flight) mass spectrometer was used to determine the concentration of all other species in solution. The carrier gas was argon at a flow rate of 1 mL min^{-1} and a run time of 40 minutes. The system was fitted with an Agilent auto-sampler and a 30 cm DB-35, (35% phenyl)-methylpolysiloxane, column. An injection volume of 10 µL was used for all samples except the calibration solutions where 1 µL was injected. Sample to sample error was approximately ±0.3 µg. From our results it is clear that a significant proportion of the different reactants tested were completely mineralised to CO_2 via intermediates that were either too short lived or at too low concentration for us to detect. CO_2 evolution was measured by sampling the gas in the headspace above the reaction and analysing the composition with a GC with a thermal conductivity detector (TCD). The system was calibrated with high purity CO_2 (99.9% purity, BOC gasses) injected in known volumes of 0.05 mL to 0.25 mL.

XP spectra were recorded from the dried powders using a Kratos Axis Ultra-DLD photoelectron spectrometer with a monochromatic Al Kα x-ray source and the "hybrid spectroscopy" mode at a pass-energy of 40 eV. The data was analysed using CasaXPS[16] with binding energies referenced to the $Ti\left(2p_{3/2}\right)$ peak of TiO_2 at 458.5 eV with an uncertainty of ~0.2 eV. Curve fits were made using Gaussian-Lorentzian (GL (30)) line-shapes.

2.4 Control reactions

In the absence of a catalyst the rate of cinnamic acid degradation under the light source and in the presence of oxygen was less than 1.3×10^{-4} s^{-1}. A no light control showed no CO_2 released in the absence of irradiation whereas, on irradiation in the presence of the mP25 photocatalyst, the degradation of the acid releases CO_2 at a rate of 1.29 μMol^{-1} s^{-1}. After 3 hours, 100% of the expected total organic carbon was released as CO_2. Under deoxygenated conditions however, the rate of CO_2 evolution was 9.8×10^{-2} μM^{-1} s^{-1} and resulted in just 8.6% of the total CO_2 being released after three hours of reaction.

3 Results

3.1 Rates of decomposition and the effect of oxygen.

On exposure to the 365 nm light source in the presence of the mP25 catalyst, a 72% decrease in cinnamic acid concentration was observed in the first 15 minutes. The initial rate of the reaction can be plotted using first order rate kinetics to give a rate constant of $1.5 \pm 0.2 \times 10^{-3}$ s^{-1}, Figure 1. A GC chromatogram recorded 20 minutes after the start of the irradiation is shown in Figure S1. The species at 11.09 minutes provided a mass spectrum with fragmentation peaks at m/z of 106.04 and 77.04 and can be attributed to the fragments $[C_6H_5CHO]$ and $[C_6H_5]^+$ identifying the molecule as benzaldehyde (**2**). A benzaldehyde calibration standard provided a matching mass spectrum and eluted at the same retention time confirming this assignment. The rate of benzaldehyde formation from cinnamic acid was measured to be very approximately 1×10^{-3} s^{-1}, only slightly less than the rate of cinnamic acid degradation and since the benzaldehyde is simultaneously degrading this is probably an underestimate. A weaker peak at an elution time of ~13.18 minutes provided a mass spectrum characterised by signals at m/z's of 120.06 and 91.06 and can be attributed to the fragments $[C_6H_5CH_2CHO]$ and $[C_6H_5CH_2]^+$ respectively arising from phenylacetaldehyde (**3**). This assignment was also confirmed with a calibration standard.

The photocatalytic decomposition of standard samples of phenylacetaldehyde and benzaldehyde (50 mg L^{-1}) were also examined to investigate the decomposition mechanism in more detail. Phenylacetaldehyde degraded at a first order rate of approximately 1.8×10^{-3} s^{-1}, however no further decomposition products were detected during its decomposition, suggesting that the products remained adsorbed on the catalyst or were reacted away to gaseous products (CO_2 & H_2O) too quickly to be detected in this experiment. Benzaldehyde decomposition occurs at a rate of approximately 0.8×10^{-3} s^{-1} with several minor products detected. These minor products were also intermittently identified in the degradation of cinnamic acid but because of their low concentration and rapid decomposition, were not observed consistently. The most significant peaks eluted at 13.0, 18.4 and 19.4 minutes with all three producing

similar mass spectra. The most probable parent mass peak was at an m/z of 122 which corresponds with hydroxybenzaldehyde [$C_6H_4(OH)CHO$]. Calibration samples for 2-hydroxybenzaldhyde and 3-hydroxybenzaldehyde eluted at 12.9 and 18.4 minutes giving the matching mass spectra. We conclude that the molecule eluting at 19.4 minutes is 4-hydroxybenzaldehyde. As direct derivatives of **2**, the 2-,3- and 4-hydroxybenzaldehyde intermediates will be referred to as **2a**, **2b** and **2c** respectively. The other significant peak in the mass spectrum was at an m/z of 93 and correlates with a fragment of hydroxybenzaldehyde minus the aldehyde group $[C_6H_4(OH)]^+$.

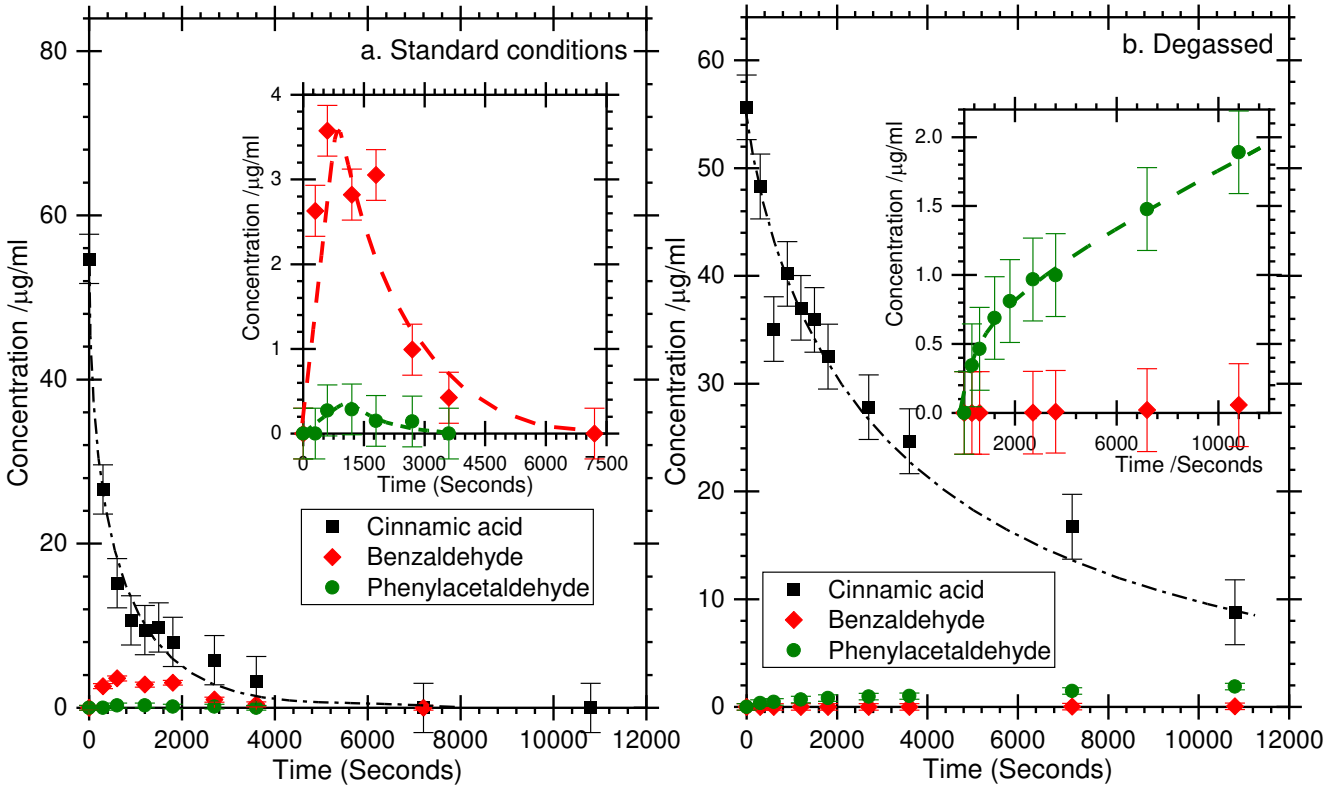

Figure 1: Concentration of cinnamic acid and its major decomposition products during photocatalytic destruction over a TiO_2 catalyst. (a) Under ambient conditions (in air at 19±1 °C); (b) In the absence of oxygen after thorough degassing with N_2 before and during the experiment. Dashed curves are drawn to guide the eye. Inset charts expand sections of the main charts.

Cinnamyl alcohol was tested as a substrate to examine how a change of the carboxyl group to an alcohol functionality would affect the degradation by mP25; studies of palladium promoted TiO_2 suggest that the alcohols are much more reactive than the acids.[17] In the present experiments, cinnamyl alcohol was seen to elute at 18.2 minutes and identified in the mass spectrum from its parent m/z of 134. Other fragments were detected at m/z of 117, 105, 91 and 77, which can be assigned as $[C_9H_{11}]$, $[C_8H_9]^+$, $[C_6H_5CH_2]^+$ and $[C_6H_5]^+$ respectively. The rate of alcohol degradation was measured to be $2.1\pm1.12\times10^{-4}$ s^{-1}, (Figure S2) significantly slower than the rate of decomposition of the carboxylic acid. The major decomposition product appeared as the second largest peak in the chromatogram, with a retention time of 17.86 minutes overlapping with the alcohol parent complex. The mass spectrum indicated a

parent mass peak at an m/z of 132 which can be attributed to cinnamaldehyde [C_9H_8O] and this is supported by signals at m/z's of 103, 93 and 77 corresponding to the fragmentation products of $[C_6H_5C_2H_2]^+$, $[C_6H_5C_1H_2]^+$ and $[C_6H_5]^+$. The concentration of cinnamaldehyde increased rapidly from the start of the reaction until ~20 minutes of illumination after which it declined at a rate similar to the rate of decomposition of the cinnamyl alcohol. By 180 minutes both the alcohol and the aldehyde were present only in trace amounts whilst benzaldehyde became the most prevalent intermediate.

3.2 The role of dissolved oxygen.

Gas phase and dissolved oxygen were eliminated from the system by purging continuously with 1 bar N_2. In all the reactions studied, the effect of removing oxygen was a dramatic decrease in reaction rate, the degradation of cinnamic acid for example was reduced by a factor of ~6 to a first order rate constant of $2.5\pm0.2\times10^{-4}$ s^{-1}, Figure 1 b. There is an accompanying change in the nature of the products of the decomposition of the acid. Benzaldehyde is the main intermediate in the presence of oxygen. It was detected only as a trace component in the oxygen free conditions whilst phenylacetaldehyde is formed, albeit in low yield, throughout the reaction in the absence of oxygen; it does not seem to decompose any further, increasing in concentration steadily throughout the 3 hours irradiation tested here, Figure 1b (inset). This is also reflected in the low levels of CO_2(g) described later (Figure 4). In the case of cinnamyl alcohol, the absence of oxygen has a similar effect, decreasing the decomposition rate to 1.8×10^{-5} s^{-1}, the cinnamaldehyde product observed in the presence of oxygen was still detected in its absence but at concentrations close to the limit of detectability.

3.3 Effect of sulfate poisoning.

Both potassium and sodium sulfates inhibit the rate of photocatalytic decomposition. We investigated the effects of 0.05 M, 0.1 M and 0.5 M of both salts and found an almost identical 5 fold decrease in the rate of cinnamic acid degradation in each case to ca. 2.9×10^{-4} s^{-1}. Illustrated in Figure 2, for the case of a K_2SO_4 concentration of 0.1 M. Removal of oxygen by purging with nitrogen reduced the rate of decomposition further to 0.94×10^{-5} s^{-1} which is similar to that at which the cinnamic acid degrades under the light source in the absence of a catalyst. (1.33×10^{-4} s^{-1}).

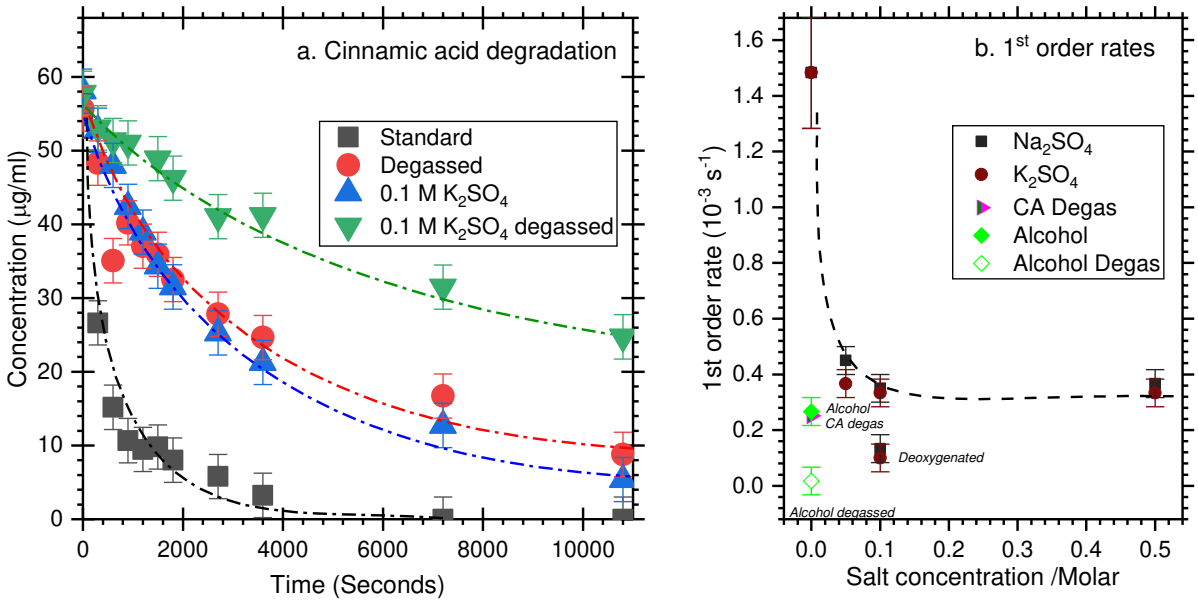

Figure 2: The effect of sulfates concentration on the rates of photocatalytic degradation of cinnamic acid. (a) Plots of the concentration of cinnamic acid against time under different conditions. (b) First order rate constants plotted as a function of potassium and sodium sulfate concentration. The rate for the degassed solution in the presence of 0.1 M sulfate are also shown.

3.3.1 Effect of sulfates on decomposition intermediates

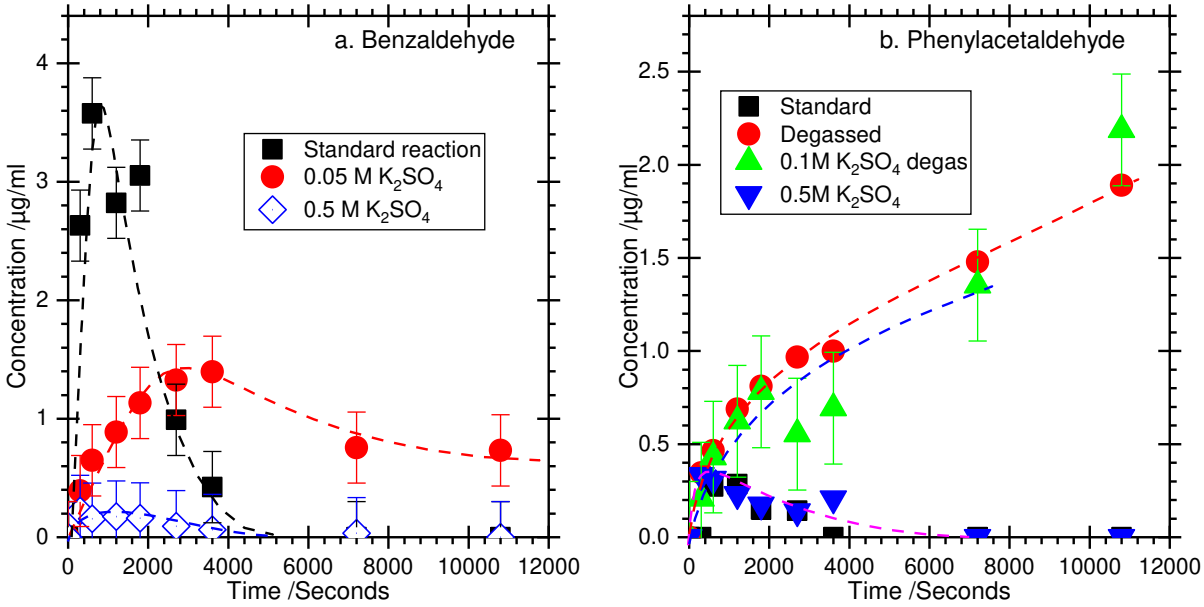

Figure 3: The effect of K_2SO_4 and oxygen on the concentrations of two cinnamic acid decomposition products: (a) benzaldehyde and (b) phenylacetaldehyde.

GC-MS data shows no new sulfated intermediates after the introduction of the aqueous sulfate ions indicating no new reaction pathways. The reduced rate of degradation of the acid is reflected in the reduced rate of benzaldehyde formation, with 0.05 M K_2SO_4 resulting in a 50% decrease. However, the point at which benzaldehyde reaches its maximum observed concentration also increases, from ~800 s in the absence of sulfate to between 3500-4500 s in the presence of 0.05 M K_2SO_4. This suggests that the rate of benzaldehyde decomposition is also reduced allowing the intermediate to persist in the system for longer as the sulfate concentration increases. At a sulfate concentration of 0.5 M and in the absence of oxygen, benzaldehyde production was almost completely inhibited. In contrast, the

concentration of phenylacetaldehyde observed in solution was not markedly different in the presence of sulfate, both in the presence and absence of oxygen, Figure 3(b).

3.4 The effect of chloride poisoning

3.4.1 Kinetic effects of potassium and sodium chloride

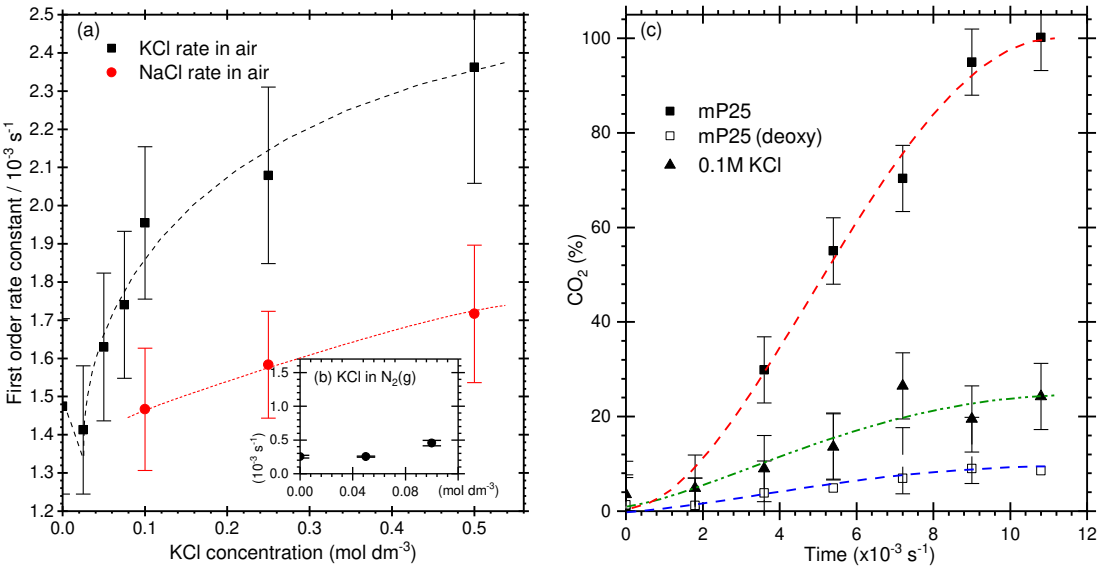

Figure 4: (a) The effect of KCl and NaCl on the rate of photocatalytic decomposition of cinnamic acid at room temperature. (b)Inset: rate of reaction in the absence of oxygen at different potassium chloride concentrations. (c) The effect of chloride and oxygen on the extent of complete photocatalytic decomposition of cinnamic acid to carbon dioxide.

The introduction of low concentrations of potassium chloride to the aqueous solution of cinnamic acid results in a decrease in the rate of cinnamic acid photocatalytic degradation, Figure 4. However, in contrast to the case of the sulfate ions, increasing the chloride concentration above 0.02 mol dm^{-3} results in an acceleration of cinnamic acid removal, the rate constant increasing from 1.5×10^{-3} s^{-1} in the absence of the chloride ion, to 2.0×10^{-3} s^{-1} in the presence of 0.1 M KCl and 2.4×10^{-3} s^{-1}, in the presence of 0.5 M KCl. NaCl demonstrated a similar promotion, although with noticeably less impact, Figure 4(a) and Figure S3. We have not investigated this aspect further, alkali metal ions are known to affect catalysts, often attributed to their influence on the availability of oxygen. In the case of the SCR process over modified TiO_2 for example, the ions act as poisons with potassium having a greater impact than sodium.[18,19] In contrast, alkali metals accelerate the oxidation of soot particles with sodium having the greater influence. Clearly, this is an area which needs further exploration.

Removal of oxygen from a solution with 0.1 M KCl present using flowing 1 bar N_2 gas resulted in rate inhibition behaviour similar to that seen under standard conditions in the absence of the salt. Control experiments in the absence of irradiation demonstrated no reaction between cinnamic acid and the chloride ion over the photocatalyst indicating that the chloride must become involved in the photocatalytic degradation reaction only after the absorption of light. However, despite the increased rate of cinnamic acid removal in the presence of chloride the

rate of carbon dioxide production is decreased, almost to the extent observed in the absence of oxygen, Figure 4(c). This suggests that the chloride ions are directing the photodegradation of the cinnamic acid down a different pathway that leads to stable side products rather than total oxidation.

3.4.2 Effect of KCl and NaCl on intermediates in the photocatalytic decomposition of cinnamic acid.

An inverse relationship between the chloride concentration and the maximum concentration reached by benzaldehyde is evident from the data in Figure 5(b). In contrast, the formation of phenylacetaldehyde (**3**) is not significantly impacted by either potassium or sodium chloride where oxygen is present occurring at concentrations of < 0.4 μg ml^{-1}. Where oxygen is absent however, **3** was detected at approximately 6 μg ml^{-1} in both 0.1M NaCl and KCl, three times higher than under similar conditions in the absence of the chloride. Four new intermediates, acetophenone (**4**), 2-chloroacetophenone (**5**), 1-(2-chlorophenyl)ethenone (**6),** and 1,2-dibenzoylethane (**7)**, were also detected via GC-MS where chloride was present, Figure 5. In a separate experiment, a reference sample of 2-chloroacetophenone (**5**) exposed to the light source in the absence of the photocatalyst generated **(6)** and **(7)** but the reverse reactions did not happen even in the presence of the catalyst. As far as we are aware this transformation has not been reported in the literature previously.

We also examined the photocatalytic oxidation of (4) in the presence of 0.5 M KCl. No chlorinated products were observed suggesting chlorine could not be added to the ring after acetephenone has formed and complete mineralisation is the preferred route. These pathways are illustrated in Figure 5. The rates of formation of the 2-chloroacetephenone and acetophenone intermediates are very rapid and the highest measured concentrations much higher than those of the benzaldehyde in the absence of the chloride ions. This perhaps reflects a slower rate of decomposition but more in-depth studies of the kinetics of these systems is clearly needed. The formation of all four intermediates was inhibited by the absence of oxygen, but their decomposition rates were unaffected by increasing chloride concentration.

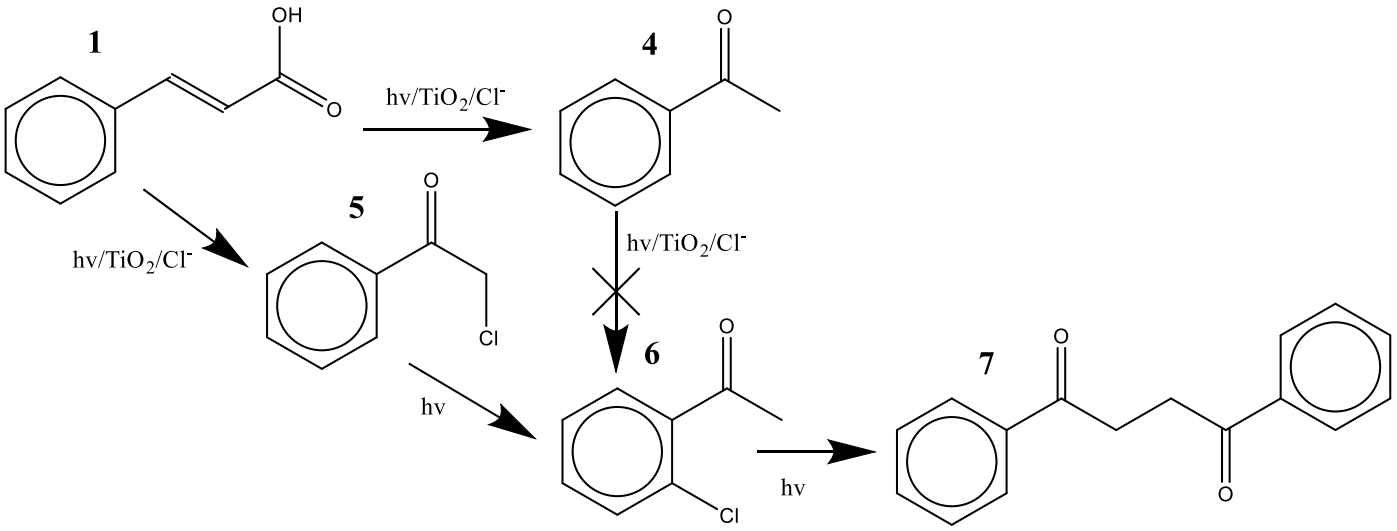

Scheme 1: The intermediates and pathways observed from the presence of up to 0.5 M KCl during the photocatalytic oxidation of cinnamic acid in the presence pf oxygen.

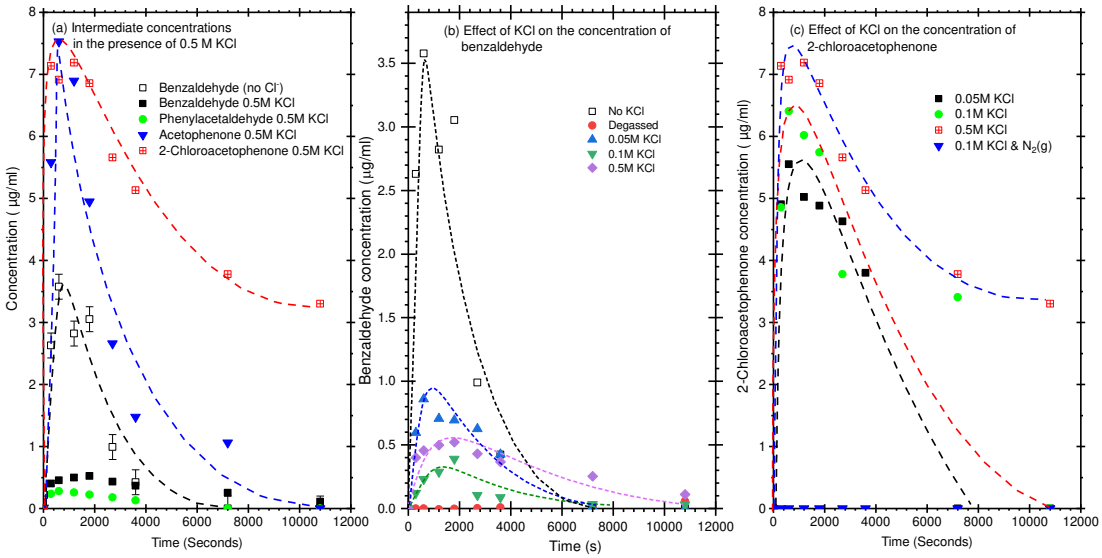

Figure 5: Effect of chloride on the photodecomposition products (a) New intermediates detected during the photocatalytic degradation of cinnamic acid in chlorinated conditions: acetophenone, **4** ; 2-chloroacetophenone **5**; 1-(2-Chlorophenyl)ethenone, **6**; 1,2-dibenzoylethane **7. (a)** Intermediate concentrations in the presence of 0.5 M KCl, the concentration of benzaldehyde under standard conditions is included for comparison; (b) The effect of KCl concentration on the concentration profile of benzaldehyde; (c) The effect of KCl concentration on the concentration profile of 2-chloroacetephenone.

3.5 Catalyst characterisation

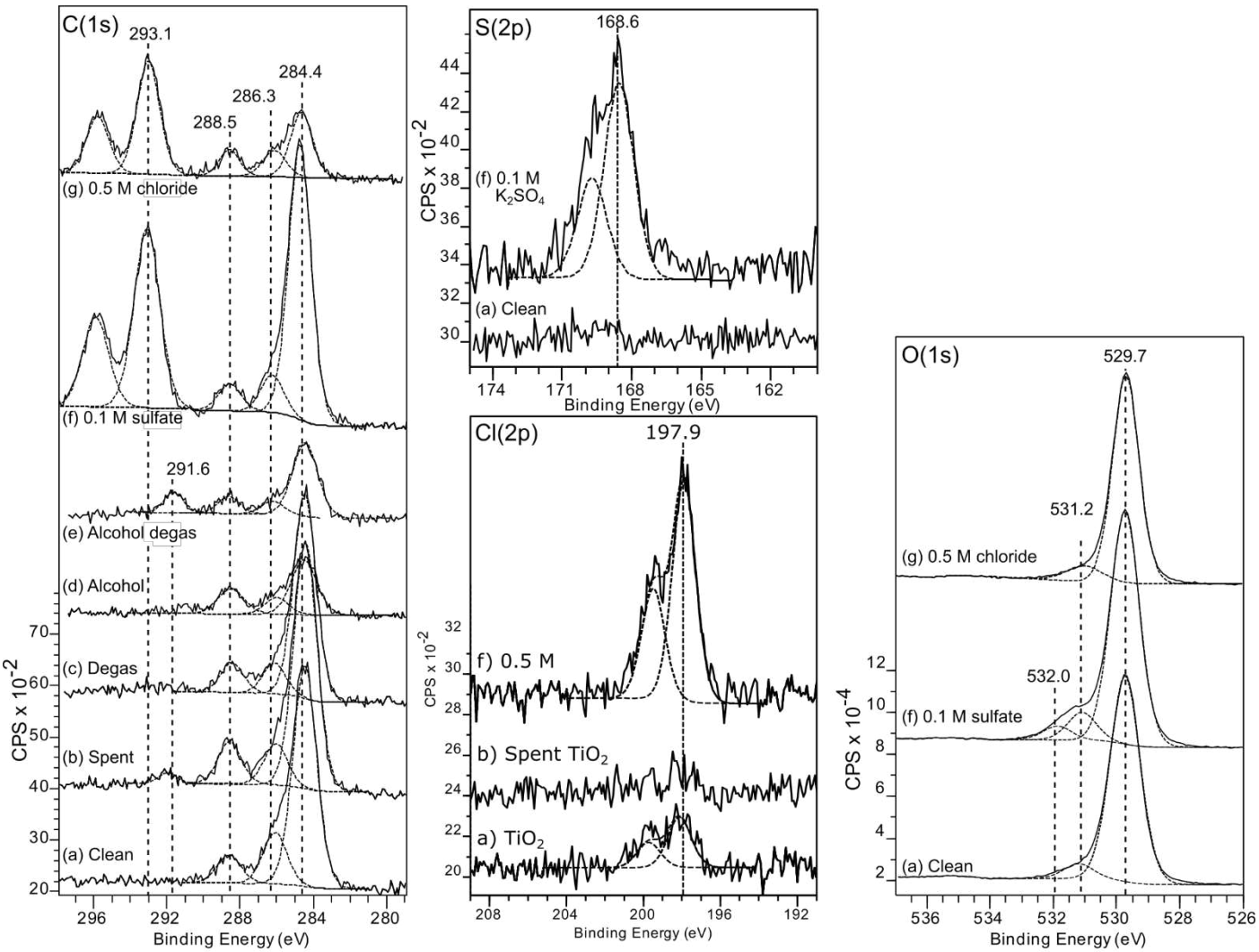

Figure 6: C(1s), O(1s), S(2p) and Cl(2p) regions of selected XP spectra of the catalysts comparing surface species before and after photocatalytic reaction in the presence of cinnamic acid and also after reaction in the absence of oxygen (degassed); (a) Fresh TiO_2; (b) After photocatalytic decomposition of cinnamic acid under standard conditions;(c) After reaction in the absence of oxygen; (d) After photocatalytic decomposition of cinnamic alcohol under standard conditions; (e) After reaction of the alcohol in the absence of oxygen; (f) After photocatalytic decomposition of cinnamic acid in the presence of 0.1 M potassium sulfate. (g) After photocatalytic decomposition of cinnamic acid in the presence of 0.5 M KCl

XP spectra of the clean and spent catalysts are compared in Figure 6. The C(1s) region shows that in addition to the usual CH_x deposition, characterised by a peak at c.a. 284.8 eV, two strong components are present at 286.3 eV and 288.5 eV. These can be tentatively assigned to C-O and C=O respectively. These three peaks are only weakly affected by the conditions of the photocatalytic degradation reaction, with neither the presence nor absence of oxygen or the presence of the sulfate ions having significant effects. A pi-pi* band indicating some extended aromatization at the surface is evident at 291.6 eV after cinnamic acid degradation in the presence of oxygen and also in the reaction of cinnamyl alcohol in the oxygen free conditions. The adsorption of the sulfate together with the potassium counter ion is evident from the $K\left(2p_{3/2}\right)$ peak in the C(1s) region at 293.1 eV, the peak at 168.6 in the S(2p) region and the associated O(1s) peak at 532.0 eV but these do not affect the other peaks in the C(1s)

region. Similarly, the presence of potassium chloride in solution is evident from the XP spectra with the $Cl\left(2p_{3/2}\right)$ at ~ 198 eV, typical of chlorides adsorbed at oxide surfaces.[20]

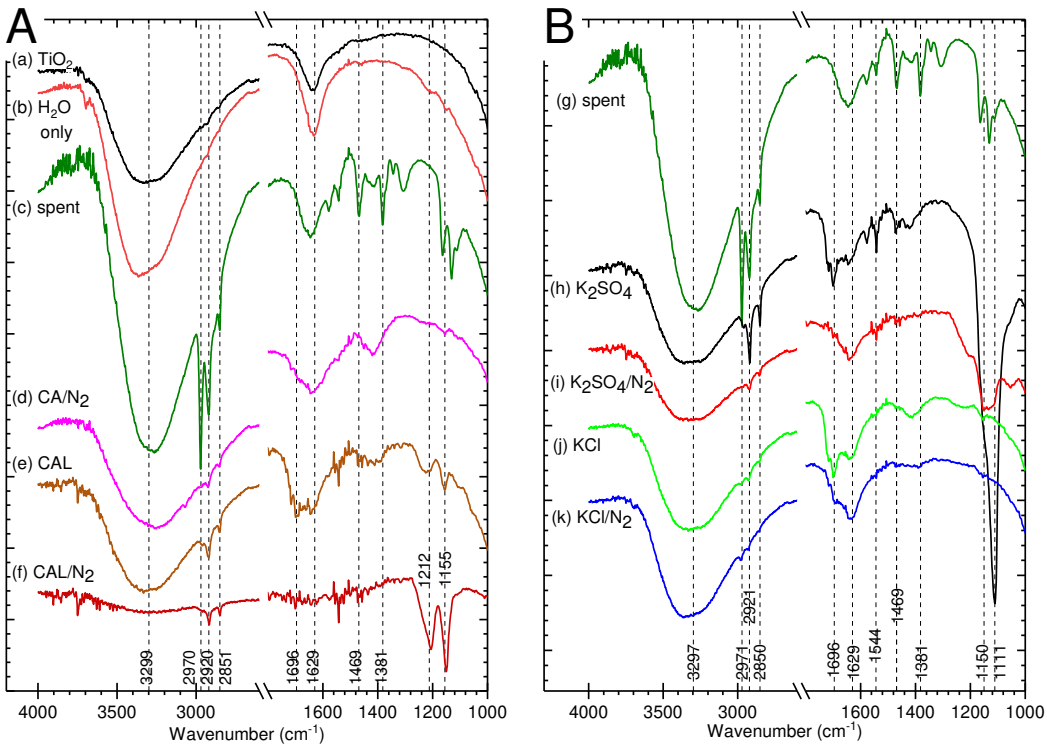

Figure 7: Fourier transform-ATR spectra of the catalysts comparing surface species before and after photocatalytic reaction in the presence of cinnamic acid (CA), cinnamic alcohol (CAL) and after reaction in the absence of oxygen (degassed, N_2) and in the presence of halide and sulfate ions:
A. (a) Fresh TiO_2; (b) Control sample of catalyst after exposure to light in pure water; (c) Spent catalyst after reaction in the presence of cinnamic acid; (d) After reaction with cinnamic acid in the absence of oxygen; (e) Catalyst after photocatalytic reaction of cinnamic alcohol; (f) After reaction with cinnamic alcohol in the absence of oxygen.
B. (g) Spent catalyst (as in (c) for comparison); (h) After reaction with cinnamic acid in the presence of 0.1 M K_2SO_4; (i) After reaction with cinnamic acid in the presence of 0.1 M K_2SO_4 and in the absence of oxygen. (j) After reaction with cinnamic acid in the presence of 0.5 M KCl; (k) After reaction with cinnamic acid in the presence of 0.5 M KCl and in the absence of oxygen.

ATR spectra of the clean TiO_2 catalyst, Figure 7, show broad vibrations at ~ 3300 and 1630 cm^{-1} attributable to adsorbed water. In addition, the no-substrate control shows a minor peak at ~ 3700 cm^{-1} due to surface hydroxyls generated by exposure of the surface to UV light. After reaction in the presence of the cinnamic acid, Figure 7(c), peaks at 2851, 2970 and 2921 cm^{-1}, assigned to the CH_3 symmetric and antisymmetric stretching and the CH_2 antisymmetric stretching modes respectively indicate the presence of hydrocarbons at the catalyst surface.[21] There is no evidence for carbonyls between ~1650 - 1850 cm^{-1}, and so the series of peaks lying between 1300 and 1580 cm^{-1} can also be assigned to vibrations of aromatic C=C, CH_3 and CH_2 groups from a range of small chain hydrocarbons such as those identified by Dang et al.[22] in the mineralisation of phenol. This correlates with the XPS evidence for aromatic groups at the surface although there is no evidence for the aromatic C-H stretching band expected ~ 3070 cm^{-1}. Similarly, the features at 1163, 1131 and 1110 cm^{-1} can be assigned to C-C stretches of these

decomposition products. Reaction in the absence of oxygen dramatically reduces the intensity of all the hydrocarbon peaks, consistent with the reduced reaction rate.

The spent catalyst from the photocatalytic decomposition of cinnamyl alcohol, Figure 7(e), gives absorptions lying between ~ 1225 and 1150 cm^{-1} which could be assigned to the C-O bending of the adsorbed alcohol. There is also clear evidence for an adsorbed carbonyl, with a peak at 1697 cm^{-1} which can be assigned to benzaldehyde as the primary intermediate still present in solution after 3 hours in this reaction. The 1697 cm^{-1} peak is absent in the deoxygenated reaction consistent with the reduced extent of reaction and this also correlates with the greater intensity seen for the peaks between ~ 1225 and 1150 cm^{-1} in the deoxygenated reaction (f) assigned to unreacted alcohol.

The introduction of the sulfate ion leads to a strong peak at 1110 cm^{-1} with a shoulder at ~1150 cm^{-1}, Figure 7(g), which can be assigned to adsorbed sulfate. In addition, peaks attributed previously to the products of the acid decomposition are evident although with weaker intensity than in the absence of the sulfate. The exception is the peak at 1697 cm^{-1}, attributed above to adsorbed benzaldehyde, and may indicate that whilst benzaldehyde is formed at the sulfated surface subsequent reactions are blocked. The presence of chloride in solution has similar effect to sulfate in that a strong peak appears at ~1697 cm^{-1}, but in this case the formation of benzaldehyde is significantly inhibited and an assignment to one of the other ketones is more likely.

4 Discussion

4.1 The mechanism of the photocatalytic decomposition of cinnamic acid

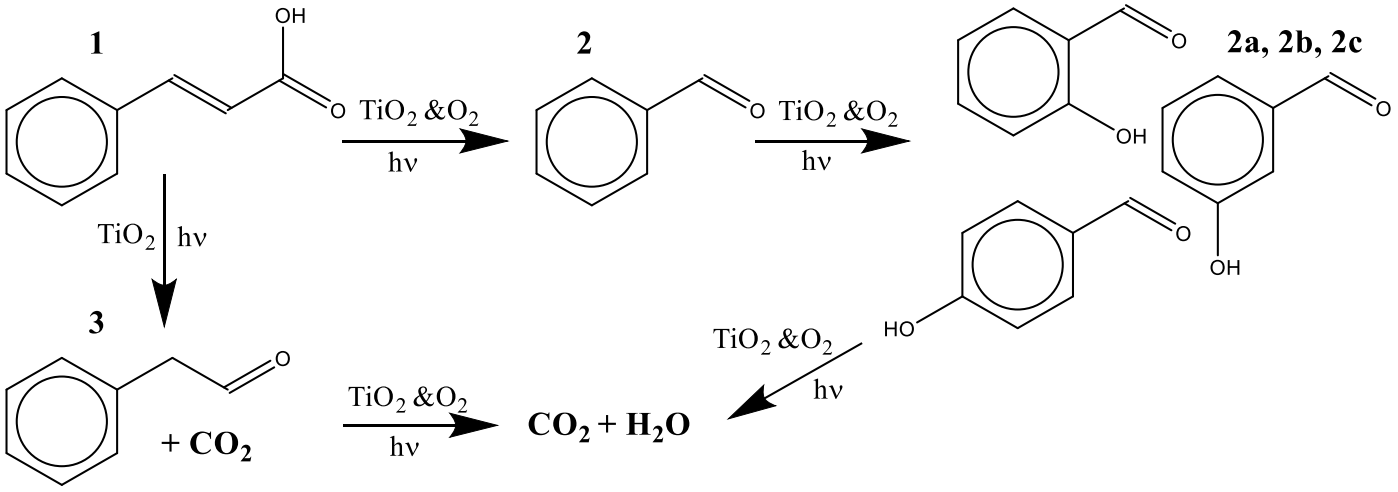

Scheme 2: The general route for the photocatalytic degradation of cinnamic acid by the titanium dioxide catalyst, showing the key intermediates

The key role played by dissolved oxygen is evident from the effects of degassing the reaction solution with flowing nitrogen. Under these conditions the rate of cinnamic acid removal is reduced by a factor of ~ 6,

benzaldehyde is no longer present as a detectable intermediate whereas phenylacetaldehyde accumulates steadily. Previous studies suggest there are likely to be two types of radical generated at the TiO_2 surface during photocatalysis: superoxide, formed via the reaction of molecular oxygen with a conduction band electron and obviously unavailable in the deoxygenated system, and hydroxyl radicals, formed from the reaction of a hydroxide ion or water molecule with a photogenerated hole and abundant in our system under all conditions (providing that e^-/h^+ recombination rates do not exceed the rate of reaction of h^+). From experiments starting from benzaldehyde, the subsequent steps in its degradation reaction probably involve hydroxyl radical attack on the ortho, para and meta positions of the aromatic ring resulting in intermediates **2a**, **2b**, and **2c**, Scheme 2, consistent with the known behaviour of hydroxyl radicals which tend to substitute aromatic rings in preference to hydrogen abstraction.[23] A second hydroxylation and subsequent ring opening is likely to follow but the species expected to evolve from here would be small molecule organics such as methanol that would be rapidly degraded to carbon dioxide and undetectable in this experiment. We do not have any data on the further photo-oxidation of the phenylacetaldehyde, **3**.

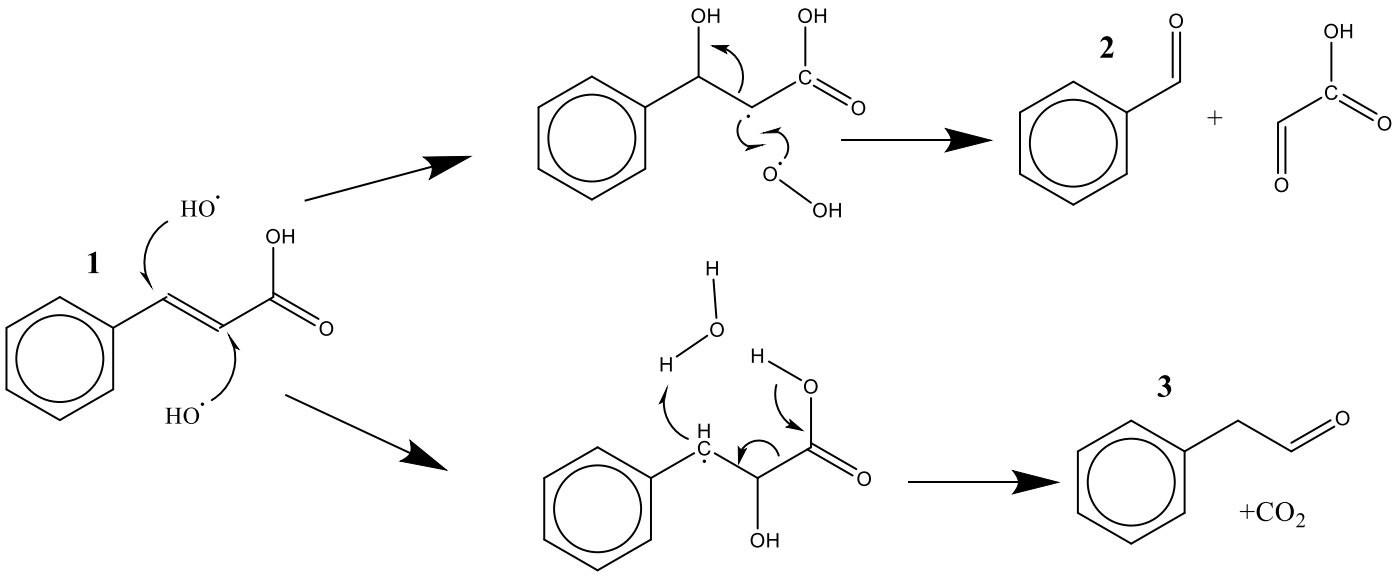

Scheme 3: Proposed mechanism depicting the formation of benzaldehyde (**2**) and phenylacetaldehyde (**3**).

The reduction in the rate of formation of benzaldehyde in the absence of oxygen implicates the superoxide radical or its protonated form, in its formation mechanism. Maeda *et al.*[24] proposed a mechanism for this reaction in which the superoxide attacks an acid already bound to the TiO_2 surface and similar mechanisms have been suggested for the superoxide led oxidation of halogenated aromatic systems and double bonds.[25] However, whilst both the FTIR and XPS do contain features that suggest a surface carboxylate, alternative schemes can be drawn without the constraint of adsorption. Scheme 3, for example shows competing pathways to products **2** and **3** arising

from attack by the hydroxyl radical on different sides of the exocyclic C=C. Hydroxylation of the position α to the carboxylic acid moiety then leads to decarboxylation to a styryl alcohol that tautomerises to product **3**, as suggested by Santos *et al.*[26] Alternatively, hydroxylation at the other side of the double bond followed by attachment of oxygen or superoxide at the radical centre and a reverse-aldol reaction cleaving the C-C bond gives **2** and O=CH-CO_2H. Note too, that the order of hydroxylation and dioxygen attack could be reversed and still give **2**.

Scheme 3 shows that the formation of **3** would result in the release of one molecule of carbon dioxide; for the conversions we observed this would result in a CO_2 volume equivalent to 11% of the total carbon present. In practice, CO_2 volumes equivalent to 9% of the total expected carbon were measured over three hours in the deoxygenated conditions, which, allowing for dissolution, is within a reasonable margin of error. It should be noted that the concentrations of **3** detected in our experiments do not match the amounts predicted if all of the CA was converted via this route but the difference can be attributed to some simultaneous degradation of **3** (via oxygen free routes in contrast to the reaction described in Scheme 2) and competition with hydroxylation of the aromatic ring which Santos et al.[26] identified as a significant route for the reaction of cinnamic acid with hydroxyl radicals generated by gamma radiolysis.

4.2 The photocatalytic degradation of cinnamyl alcohol

Photocatalytic oxidation of the cinnamyl alcohol in the presence of oxygen, generates the corresponding aldehyde in the first instance, with benzaldehyde (**2**) forming subsequently. Cinnamyl alcohol can be readily oxidised to cinnamaldehyde and subsequently to cinnamic acid upon exposure to air[27] but because the acid does not readily appear in GC-MS, its presence was not tested for in these reactions. Benzaldehyde forms slowly from the beginning of the irradiation and accumulates throughout the reaction but it we have not ascertained whether it forms directly from cinnamyl alcohol or one of its oxidation products. Rossi *et al*.[28] found that, over a Ag-Au catalyst, in the presence of a radical trap, cinnamyl alcohol was selectively oxidised to cinnamaldehyde whereas benzaldehyde was the main product in the absence of the radical trap suggesting it forms via a radical cleavage of the C=C bond of cinnamaldehyde in solution. In the absence of oxygen, there was very little photocatalytic oxidation of the cinnamyl alcohol.

4.3 The effect of aqueous sulfate ions on the photocatalytic degradation mechanisms

The presence of sulfate in concentrations as low as 0.05 M inhibits the photocatalysed degradation of cinnamic acid and two different effects could be responsible: blocking of surface sites or scavenging of hydroxyl radicals.

Figure 2, shows that the rate of formation of **2** is reduced by the presence of sulfate ions but not its decomposition rate whilst the *formation* of **3** is unaffected by sulfate but its *removal* is blocked, allowing **3** to build up in concentration. These effects rule out hydroxyl radical scavenging by sulfate as a significant factor since it would be expected to impact both the removal of **2** and the formation of **3**. On the other hand, sulfate's role as a surface site blocker is supported by the post-reaction XPS and IR data both of which show sulfate adsorption on the catalyst surface. Where sulfate is present but oxygen absent, the rate of cinnamic acid degradation is reduced to the catalyst free rate with the degradation pathway that produced **2** completely blocked. However, the formation of **3** is unaffected showing that the pathway to **3** does not rely on either the superoxide or access to the surface. This is consistent with the hydroxyl radical driven process proposed in Scheme 2 occurring in solution.

4.4 The effect of aqueous chlorides

The increased rate of removal of cinnamic acid in the presence of chloride and the detection of chlorine substituted products, suggest that reactive chlorine species are providing alternative pathways for the decomposition of the acid, the reduction in CO_2 yield however indicates that the chloride also inhibits complete mineralisation.

Reaction 1:	$Cl^- + h^+ \rightarrow Cl^\bullet$	$k_1 = 1\times10^7\ M^{-1}\ s^{-2}$
Reaction 2:	$HO^\bullet + Cl^- \rightarrow ClOH^{\bullet-}$	$k_2 = 4.3\times10^9\ M^{-1}\ s^{-1}$
Reaction 3:	$ClOH^{\bullet-} \rightarrow HO^\bullet + Cl^-$	$k_3 = 6.1\times10^9\ s^{-1}$
Reaction 4:	$ClOH^{\bullet-} \rightarrow Cl^\bullet + OH^-$	$k_4 = 23\ s^{-1}$
Reaction 5:	$ClOH^{\bullet-} + H^+ \rightleftarrows Cl^\bullet + H_2O$	$k_5 = 2.1\times10^{10}\ M^{-1}\ s^{-1}$ $k_{-5} = 1.3\times10^3\ s^{-1}$
Reaction 6:	$ClOH^{\bullet-} + Cl^- \rightarrow OH^- + Cl_2^{\bullet-}$	$k_9 = 1.0\times10^5\ M^{-1}\ s^{-1}$
Reaction 7:	$Cl^\bullet + Cl^- \rightarrow Cl_2^{\bullet-}$	$k_{10} = 6.5\times10^9\ M^{-1}\ s^{-1}$ $k_{-10} = 1.1\times10^5\ s^{-1}$

Table 1: Pathways for chloride ions and radicals in aqueous solution. Data taken from references[29–31]

Chloride ions are known to form reactive species readily through several mechanisms, Table 1,[29–31] with $Cl^\bullet$ and $Cl_2^{\bullet-}$ the most reactive species. $Cl^\bullet$ reacts with oxygenated hydrocarbons around 5 times faster than the dichloride

radical,[32–34] and orders of magnitude faster than $HO^{\bullet}$ in the gas phase[35] and is therefore likely to be the active species in this case.

The products acetophenone **(4)**, and 2-chloroacetophenone **(5)** which appear in the presence of chloride ions, Figure 5, have similar dependencies on dissolved oxygen as **2**, and similar placements of oxygen, suggesting they both arise from the chlorine atom intercepting an intermediate ***after*** the attack of the superoxide. A number of possibilities could be suggested but we have no direct experimental evidence to identify the reaction pathway that leads to products **4**, **5**, **6** and **7** and so we will not speculate here on the actual path. As in the case of sulfated media, the presence of the chloride exhibits no influence on the production of **3** under oxygenated conditions but in deoxygenated conditions a very distinct increase in the production of **3** was found. These observations are consistent with Scheme 3, in which **3** is formed by hydroxyl radicals and does not compete with the chloride based mechanisms.

5 Conclusions

A combination of GC-MS and UV-Vis spectroscopy has revealed details of the reaction mechanism for the photocatalytic decomposition of cinnamic acid in aqueous solution over a P25, TiO_2 catalyst. The principal pathway involves attack at the alkene group by a super oxide radical, generating benzaldehyde as the main intermediate. Benzaldehyde undergoes attack by hydroxyl radicals, generating OH substituted intermediates that are subsequently decomposed to CO_2 via a series of steps that occur too quickly for us to identify. An alternative reaction pathway, in the absence of dissolved oxygen, is suggested to occur via hydroxylation of the carbon α to the carboxylic acid, followed by decarboxylation to give styryl alcohol which tautomerises to phenylacetaldhyde.

The presence of sulfate in solution inhibits the dioxygen radical mechanism significantly reducing the rate of cinnamic acid decomposition but does not introduce any further reaction pathways. The sulfate does not impact the hydroxyl radical mediated route to phenylacetaldhyde nor does it inhibit the subsequent decomposition of phenylacetaldhyde however, the rate of benzaldehyde photodecomposition is reduced perhaps suggesting that the latter requires access to the surface whereas the phenylacetaldhyde decomposition route does not.

In contrast to the sulfate, the presence of chloride in solution leads to an acceleration of the rate of removal of cinnamic acid. Under these conditions several chlorine substituted products are generated including acetophenone, 2-chloroacetophenone, 1-(2-chlorophenyl)ethenone, and 1,2-dibenzoylethane. These products suggest the formation of radical chlorides that intercept intermediates in the catalytic oxidation of the cinnamic acid diverting

the path from full decomposition into the formation of undesirable side products. Our results strongly demonstrate the importance of screening for potentially harmful side products where photocatalysis is used to remove water borne contaminants in the presence of halide ions; both the chlorinated products we have detected are toxic,[36,37] with 2-chloroacetophenone, which is acutely toxic through inhalation, skin contact and ingestion, being particularly concerning.

6 Acknowledgements

This work carried out as part of the PCATDES project funded by European Union's Seventh Framework Programme under Grant Agreement N. 309846. XPS data collection was performed at the EPSRC National Facility for XPS ("HarwellXPS") under contract No. PR16195.

7 References

1 Oil Palm & The Environment (updated March 2014), http://www.mpob.gov.my/palm-info/environment/520-achievements#Growthoftheindustry, (accessed 11 February 2019).
2 P. Jamal, Z. M. Idris and M. Z. Alam, *Food Chem.*, 2011, **124**, 1595–1602.
3 D. O. Edem, *Plant Foods Hum. Nutr.*, 2002, **57**, 319–341.
4 L. Dogliotti and E. Hayon, *J. Phys. Chem.*, 1967, **71**, 2511-+.
5 J. Wiszniowski, D. Robert, J. Surmacz-Gorska, K. Miksch and J. V. Weber, *Int. J. Photoenergy*, 2003, **5**, 69–74.
6 U. I. Gaya, A. H. Abdullah, Z. Zainal and M. Z. Hussein, *J. Hazard. Mater.*, 2009, **168**, 57–63.
7 J. Mendez-Diaz, M. Sanchez-Polo, J. Rivera-Utrilla, S. Canonica and U. von Gunten, *Chem. Eng. J.*, 2010, **163**, 300–306.
8 M. Makita and A. Harata, *Chem. Eng. Process.-Process Intensif.*, 2008, **47**, 859–863.
9 K.-H. Wang, Y.-H. Hsieh, C.-H. Wu and C.-Y. Chang, *Chemosphere*, 2000, **40**, 389–394.
10 A. Piscopo, D. Robert and J. V. Weber, *Appl. Catal. B Environ.*, 2001, **35**, 117–124.
11 S.-Y. Yang, Y.-X. Chen, L.-P. Lou and X.-N. Wu, *J. Environ. Sci.*, 2005, **17**, 761–765.
12 R. Yuan, S. N. Ramjaun, Z. Wang and J. Liu, *Chem. Eng. J.*, 2012, **192**, 171–178.
13 B. Ohtani, O. O. Prieto-Mahaney, D. Li and R. Abe, *J. Photochem. Photobiol. Chem.*, 2010, **216**, 179–182.
14 A. Sergejevs, C. T. Clarke, D. W. E. Allsopp, J. Marugan, A. Jaroenworaluck, W. Singhapong, P. Manpetch, R. Timmers, C. Casado and C. R. Bowen, *Photochem. Photobiol. Sci.*, 2017, **16**, 1690–1699.
15 C. Casado, R. Timmers, A. Sergejevs, C. T. Clarke, D. W. E. Allsopp, C. R. Bowen, R. van Grieken and J. Marugán, *Chem. Eng. J.*, 2017, **327**, 1043–1055.
16 N. Fairley, *CasaXPS Manual: 2.3.15 Spectroscopy*, Casa Software Ltd, 2009.
17 M. Bowker, C. Morton, J. Kennedy, H. Bahruji, J. Greves, W. Jones, P. R. Davies, C. Brookes, P. P. Wells and N. Dimitratos, *J. Catal.*, 2014, **310**, 10–15.
18 R. Guo, Q. Wang, W. Pan, W. Zhen, Q. Chen, H. Ding, N. Yang and C. Lu, *Appl. Surf. Sci.*, 2014, **317**, 111–116.
19 L. Chen, J. Li and M. Ge, *Chem. Eng. J.*, 2011, **170**, 531–537.
20 H. Altass, A. F. Carley, P. R. Davies and R. J. Davies, *Surf. Sci.*, 2016, **650**, 177–186.
21 Z. Topalian, B. I. Stefanov, C. G. Granqvist and L. Österlund, *J. Catal.*, 2013, **307**, 265–274.
22 T. T. T. Dang, S. T. T. Le, D. Channei, W. Khanitchaidecha and A. Nakaruk, *Res. Chem. Intermed.*, 2016, **42**, 5961–5974.
23 M. Anbar, D. Meyerstein and P. Neta, *J. Phys. Chem.*, 1966, **70**, 2660–2662.
24 H. Maeda, H. Nakagawa and K. Mizuno, *J. Photochem. Photobiol. Chem.*, 2007, **189**, 94–99.
25 H. Sugimoto, S. Matsumoto and D. T. Sawyer, *J. Am. Chem. Soc.*, 1987, **109**, 8081–8082.
26 P. M. P. Santos and A. J. S. C. Vieira, *J. Phys. Org. Chem.*, 2013, **26**, 432–439.
27 I. B. Niklasson, T. Delaine, M. N. Islam, R. Karlsson, K. Luthman and A.-T. Karlberg, *Contact Dermatitis*, 2013, **68**, 129–138.
28 J. C. S. Costa, P. Corio and L. M. Rossi, *Nanoscale*, 2015, **7**, 8536–8543.
29 G. Jayson, B. Parsons and A. Swallow, *J. Chem. Soc.-Faraday Trans. I*, 1973, 1597–1607.
30 J. E. Grebel, J. J. Pignatello and W. A. Mitch, *Environ. Sci. Technol.*, 2010, **44**, 6822–6828.

31 U. Klaning and T. Wolff, *Berichte Bunsen-Ges.-Phys. Chem. Chem. Phys.*, 1985, **89**, 243–245.
32 H. W. Jacobi, F. Wicktor, H. Herrmann and R. Zellner, *Int. J. Chem. Kinet.*, 1999, **31**, 169–181.
33 F. Wicktor, A. Donati, H. Herrmann and R. Zellner, *Phys. Chem. Chem. Phys.*, 2003, **5**, 2562–2572.
34 G. V. Buxton, M. Bydder, G. A. Salmon and J. E. Williams, *Phys. Chem. Chem. Phys.*, 2000, **2**, 237–245.
35 L. Nelson, O. Rattigan, R. Neavyn, H. Sidebottom, J. Treacy and O. Nielsen, *Int. J. Chem. Kinet.*, 1990, **22**, 1111–1126.
36 PubChem, 2-Chloroacetophenone, https://pubchem.ncbi.nlm.nih.gov/compound/10757, (accessed 2 March 2020).
37 PubChem, 1-(2-Chlorophenyl)ethanol, https://pubchem.ncbi.nlm.nih.gov/compound/26082, (accessed 2 March 2020).